Chapter 13

The "large angle" analysis

The so called "large angle" region of the HARP detector is the zone covered just by the TPC and the barrel RPCs. In this region, the angular range for particles emerging from the origin is from 0.38 to 2.47 radians as sketched in figure 13.1. This angular range is however slightly modified for runs with 100% interaction length targets.

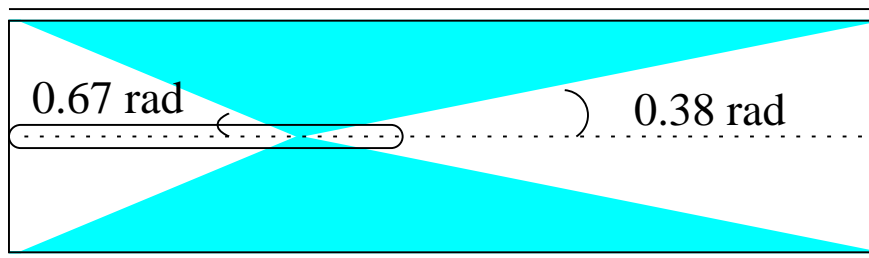An analysis is performed, discussed below, which uses information coming from the

Figure 13.1: The "large angle" region.

beam instrumentation, the TPC, the barrel RPCs and the Inner Trigger Cylinder.

13.1 Tantalum target at $3\,\text{GeV/c}$ beam momentum

The first target material analysed is the ^{73}Ta for a beam momentum of $3\,\text{GeV/c}$. Data obtained in the 2001 run with 2% and 100% interaction length target were collected. They were reconstructed using a preliminary version of the software, available in May 2002. Since then, several improvements to the various algorithms were implemented but, unfortunately, no production with the new reconstruction code was possible at the time of writing and and there is not yet possibility to identify particles.

The analysis is focused on interactions caused by protons. The first step is hence their selection, which is particularly important because, at low momentum, the T9 beam is highly contaminated by electrons and other particles, as shown in figure 9.2. At $3\,\text{GeV/c}$, the beam protons are identified by their time-of-flight while electrons are vetoed by the beam Cherenkov counter "A".

13.1.1 Over lay interactions

At low momentum, *out-of-time* interactions are often observed. They are produced by the interaction of a beam particle which arrives inside the 30μs time window of the beam particle that triggered the data acquisition.

These tracks are reconstructed with an incorrect z position because of their time offset and are cut in the analysis requiring an RPC signal matching the track extrapolated from the TPC.

13.1.2 Preliminary cuts

A set of preliminary cuts is applied to select tracks:

- there must be an ITC hit for the event, what defines a large angle interaction

- no numerical error nor error flag should be associated with the track

- the tracks must have at least 10 hits to ensure an accurate fit

- the particles have $P_t > 10\,\mathrm{MeV/c}$, in order to reject passing through particles and noise

- there is a TPC-RPC match to cut out-of-time tracks and to ensure a greater accuracy

- the transverse momentum should not exceed $1\,\mathrm{GeV/c}$ and the longitudinal momentum should be in the range -1-2 $\mathrm{GeV/c}$ because of kinematical constraints

The last cut is derived from the hypothesis of an incoming proton interacting with a proton at rest and yielding a final state with a proton at rest and a proton and a pion sharing the remaining energy.

13.2 Impact point reconstruction

The impact point of the selected tracks is reconstructed. The plots in figure 13.2 show the absolute value of the impact parameter d_0 and the z coordinate of the impact point for the thin and thick target.(The dimensions of the thin target are $30\,\mathrm{mm}$ diameter in $x-y$ and $2.2\,\mathrm{mm}$ in z. It is located downstream of the origin of the axis. The thick target has the same diameter of the thin one and a length of $170.1\,\mathrm{mm}$ in z. It is centred on $z{=}0$.)

The left plots in the figure show that the impact parameter distribution has the same width for the thin and thick target, as expected. There is an excess in the region of $d_0 \approx 30\,\mathrm{mm}$, discussed below.

The z distributions reproduce the target dimensions. The small peak visible at around $300\,\mathrm{mm}$ in the thin target data is due to interactions in the end-cup of the Stesalit field cage. It is not visible for the thick target data since is masked by a greater background.
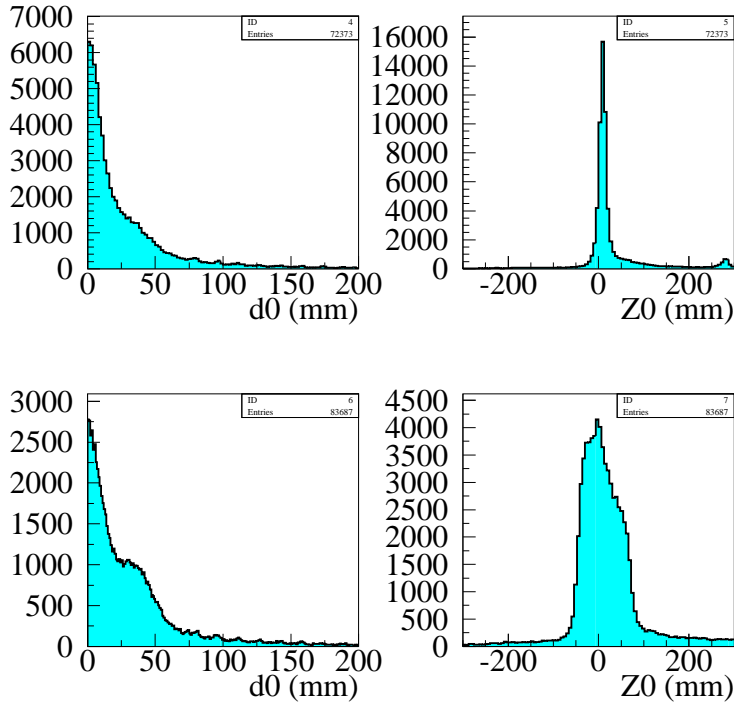
Figure 13.2: Absolute value of the radial coordinate and longitudinal coordinate of the impact point for proton collisions on thin (upper) and thick (lower) Ta target for a 3 GeV/c beam momentum.

13.2.1 Investigation on the impact point shape

A closer look at the d_0 distribution with its sign, shows that the anomalous excess of events appears for negative d_0 only (figure 13.3).
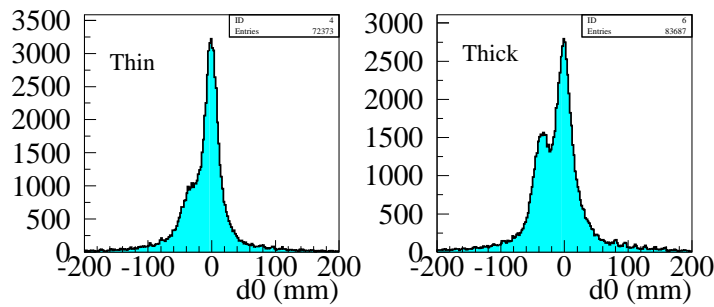

Figure 13.3: Impact parameter for thin and thick Ta target data at 3 GeV/c.

Additional information can be obtained by looking at the correlation between d_0 and the transverse momentum presented in figure 13.4.
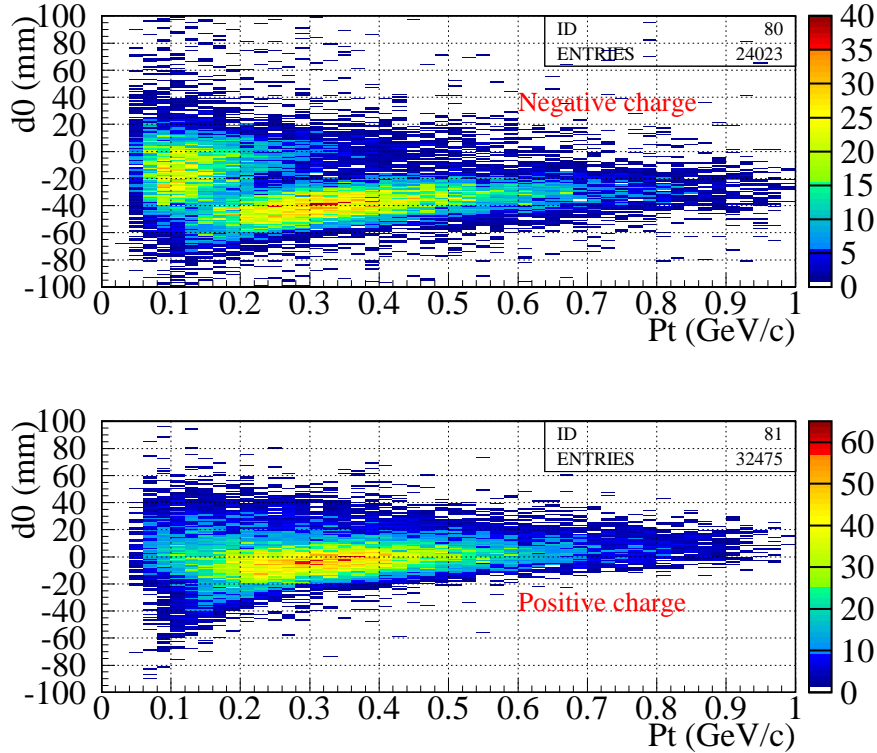

Figure 13.4: Correlation between the impact parameter and the transverse momentum for negative (upper) and positive (lower) particles.

For negative particles, two distinct zones are visible, one symmetric around $d_0 = 0$ with relatively low p_t and the other asymmetric towards negative d_0 values and at larger p_t.

For positive particles, a single zone is observed.

The effect may be interpreted as follows. The majority of the events occurs around $d_0 = 0$, both for positive and negative charges. However, for large transverse momenta the track curvature is small and the experimental resolution can lead to charge confusion, *i.e.* the negative charges might be identified as positive and vice-versa.
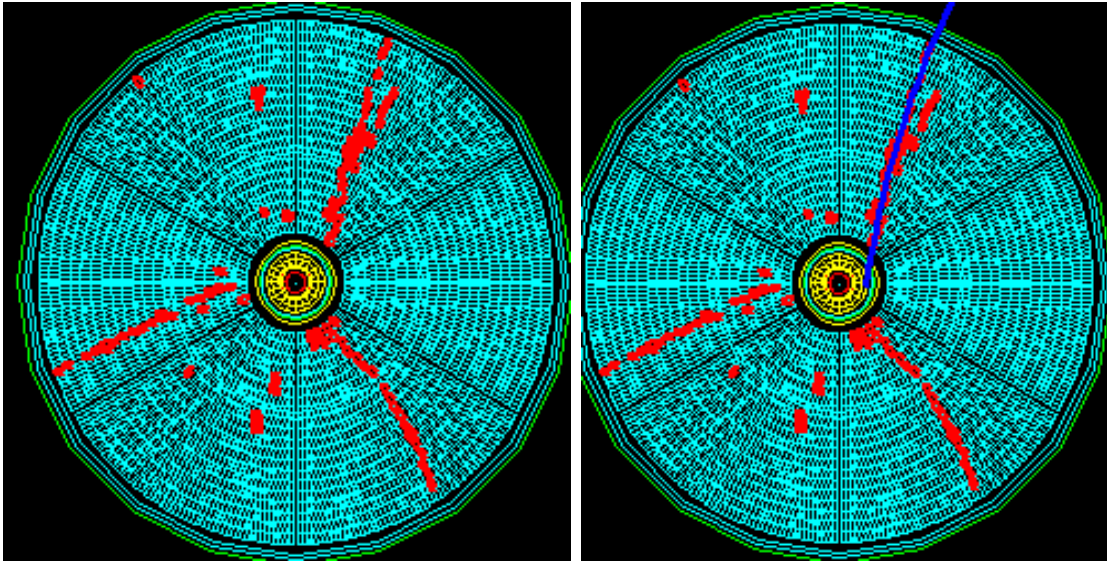
Figure 13.5: Example of events showing the charge assignment problem.

At the same time, the wrong curvature shifts the events from small values of d_0, irrespectively of its sign, to large and negative values. An example of event showing this charge assignment problem is shown in figure 13.5. This happens symmetrically in the two charge cases, however, given the unbalance between the two distributions, the contamination from positive charges on the negative charge distribution is visible, while the opposite is not true. The excess of events in fact is visible only in the negative charge case, while , to a first approximation, the one for the positive charge can be considered as the real one.

Figure 13.6 shows the d_0 distributions separately for positive and negative particles and for different transverse momentum slices. At low momentum, an excess on the negative d_0 side is visible both for positive and negative particles. It can be due to e^+e^- pairs generated by photon conversions on the target surface. The tracks corresponding to these pairs have in fact negative impact parameter. Going at higher momenta, where the track reconstruction is more difficult due to the little sagitta
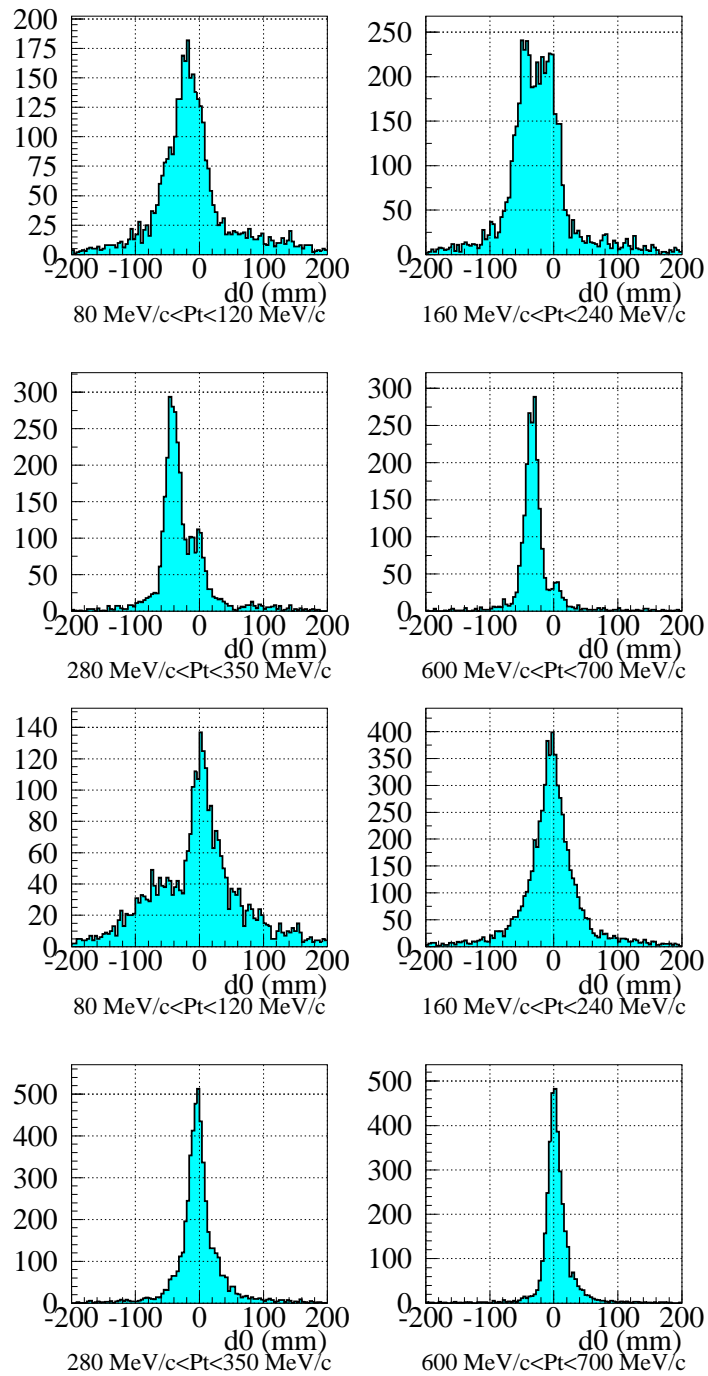
Figure 13.6: Impact parameter at different P_t values for negative (upper 4 plots) and positive (lower 4 plots) particles.

194

value, for the negative particles the peak of the tracks with wrong charge assignment and negative impact parameter becomes more and more high. The effect is not clearly visible for the positive particles given the already mentioned unbalance of the relative abundances.

To remove this systematic effect, only tracks with low absolute values of the impact parameter are considered in the following, and, in particular, particles with $0\,\mathrm{mm} < d_0 < 2\,\mathrm{mm}$ are retained. In this way, tracks with wrong charge assignment are rejected without yielding any bias in the momentum distributions.

Applying this cut, the distribution of z reported in the plots 13.7 are obtained. There is no substantial difference with the result obtained before the cut on d_0, what proves that there is no correlation between the z coordinate of the impact point and possible charge assignment confusion.

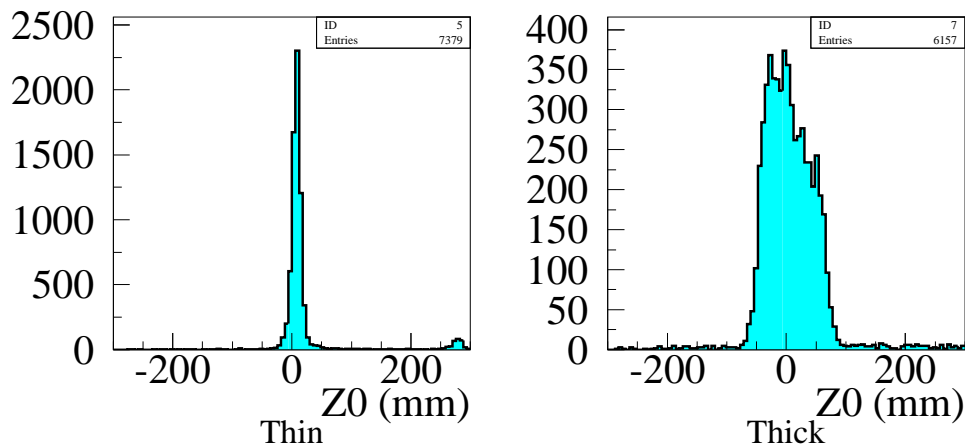For further analysis, an additional selection on the z coordinate of the impact point

Figure 13.7: z coordinate of the impact point after the cut on d_0.

is applied, to cut tracks not originating from the target region and to eliminate the background.

13.3 Momentum distributions

The transverse momentum distributions for the thin and thick targets are displayed in figure 13.8. The mean p_t is around $365\,\mathrm{MeV/c}$ for both target length.

The maximum kinematically allowed p_t is of about $0.7\,\mathrm{GeV/c}$ but a small fraction of the events is beyond this value, compatible with the error in the momentum reconstruction of about $200\,\mathrm{MeV/c}$.

The transverse momentum region below $100\,\mathrm{MeV/c}$ is more populated by negative particles than positive. Particles with valence antiquarks must originate from gluon
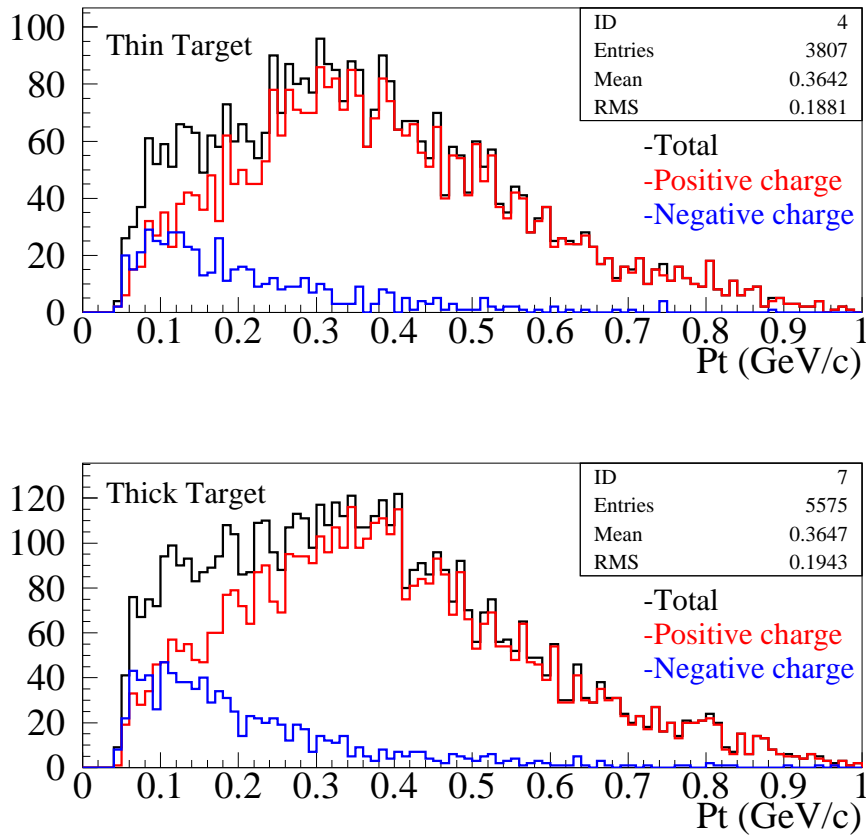

Figure 13.8: Transverse momentum distributions with the Tantalum targets and beam momentum of $3\,\mathrm{GeV/c}$.

radiation whose emission probability is peaked at low energy. Gluons, in turn, convert into $q\bar{q}$ pairs that give rise to soft, charge symmetric particles. In addition, π_0 decaying into two photons may create electron-positron pairs that contribute to restore a charge symmetry. The two cases will be distinguished when it will be possible the use of the RPCs to identify the particles by time-of-flight. In addition, in the momentum region below $100\,\mathrm{MeV/c}$, the TPC should permit electron/pion separation via dE/dx measurements.

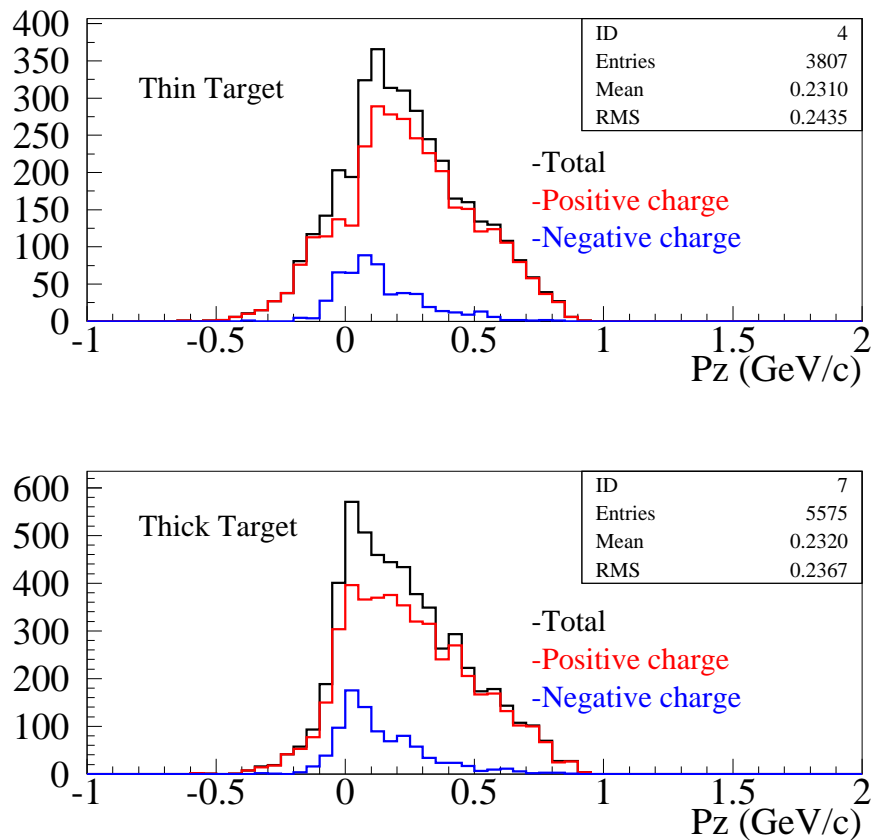Longitudinal momentum distributions are shown in figure 13.9. The maximum visible

Figure 13.9: Longitudinal momentum distributions with Tantalum target and a proton beam momentum of $3\,\mathrm{GeV/c}$.

p_z is restricted by the request of large angle interaction that forbids particles in the

forward direction within a cone of ± 0.38 radians around the beam line. Therefore, the kinematic limit of the order of $1.7\,\mathrm{GeV/c}$ can not be reached. Indeed, the kinematic limit compatible with the angular cut turns out to be around $1.1\,\mathrm{GeV/c}$. In the backward direction, the limit for negative longitudinal momentum is $\approx 250\,\mathrm{MeV}$. The observed distributions are in good agreement with these kinematic limits.

The charge asymmetry increases with the longitudinal momentum because of the onset of the leading particle effect that gives more momentum to particles with the same charge of the projectile. This effect would be clearly visible including the forward region in the acceptance.
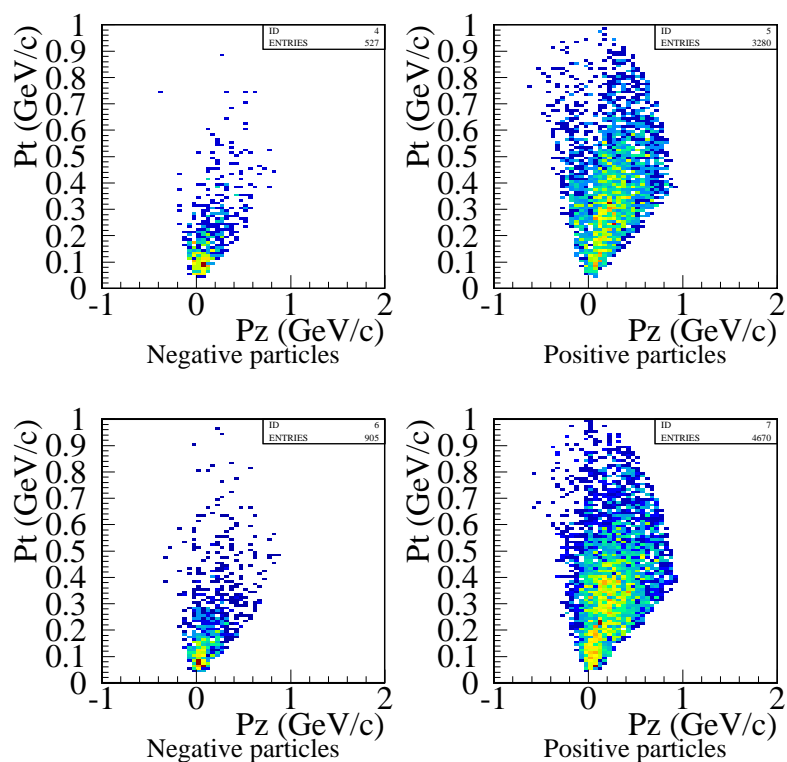

Figure 13.10: Correlation between transverse and longitudinal momentum obtained with the thin (upper plots) and the thick (lower plots) Tantalum target and a proton beam momentum of $3\,\mathrm{GeV/c}$. Positive and negative particles are separated.

The histograms in figure 13.10 show the $p_t - p_z$ correlation for positive and negative particles and are bounded by the large angle cuts that are of the form $p_t/p_z < C$, where C is a different constant for the forward and backward zone. The plots indicate for the forward region $C \approx 0.4$ and for the backward region $C \approx 1.0$, in agreement with expected values. The plots indicate a mild correlation.

13.4 Positive to negative particle ratio

The positive to negative particle ratio summed over all momenta is 6.2 for the thin target and 5.2 for the thick one. The detailed momentum distributions show that it is a function of the particles momenta that tends to 1 for soft particles. The thickness dependence can be attributed to the re-interaction that tends, for thicker targets, to equalise negative and positive charges in the final state.

13.5 K2K target

K2K [89] is a long baseline experiment which aims to confirm the growing evidence of neutrino oscillations. A proton beam of $12\,\mathrm{GeV}$ energy is shone on an Al target. The pions produced in the collision decay into muons and ν_μ, which are detected in a near detector, located approximately $250\,\mathrm{m}$ downstream the target station. The ν_μ beam travels $250\,\mathrm{km}$ to the SuperKamiokande detector, where the disappearance of ν_μ is investigated (figure 13.11). In K2K the pion yield in the energy region below $1\,\mathrm{GeV/c}$ is estimated at present using a Monte Carlo. Clearly the experiment would benefit of a direct measurement of the pion production cross section. For that reason, aluminium targets similar to that used in K2K and of other various thicknesses were investigated in the HARP experiment, at a beam momentum of $12.9\,\mathrm{GeV/c}$.
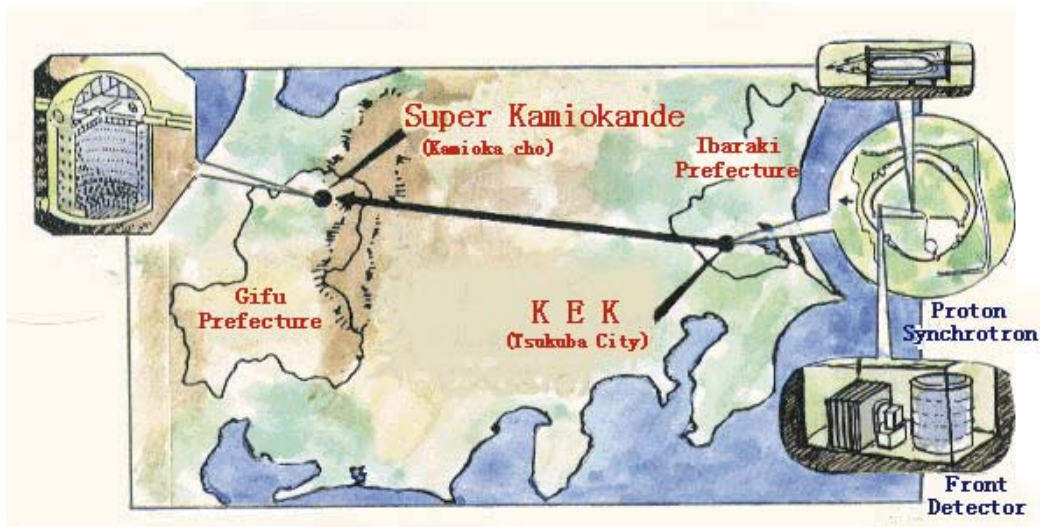
Figure 13.11: Outline of the K2K experiment.

13.6 The analysis of the K2K data

An analysis is reported on "K2K data" collected during August 2002 and based on an improved version of the reconstruction software with respect to the Tantalum case, albeit still incomplete and without particle identification.

Two targets are considered, a thin one, of 2% interaction length, and a thick one, of 100% interaction length. As in the Tantalum case, the thin target position in the HARP experiment is downstream of the origin while the thick one is centred in the origin. The target length are 7.9 mm and 394.4 mm, respectively, while their diameter is 30 mm.

Beam protons are selected vetoing signals in both beam Cherenkov counters.

The same set of preliminary cuts used for the Tantalum is applied, with the exception of those on the transverse and longitudinal momenta. To take into account the beam momentum of 12.9 GeV/c, the kinematical constraints read:

- transverse momentum below 2.5 GeV/c

200

- longitudinal momentum in the range $-1 \div 6\,\mathrm{GeV/c}$

The cut on the longitudinal momentum is not very strict and considers the forbidden forward and backward angles.

13.6.1   Impact point reconstruction

Figure 13.12 shows the absolute value of the radial and the longitudinal coordinates of the impact point for the two different target thiknesses. The impact parameter
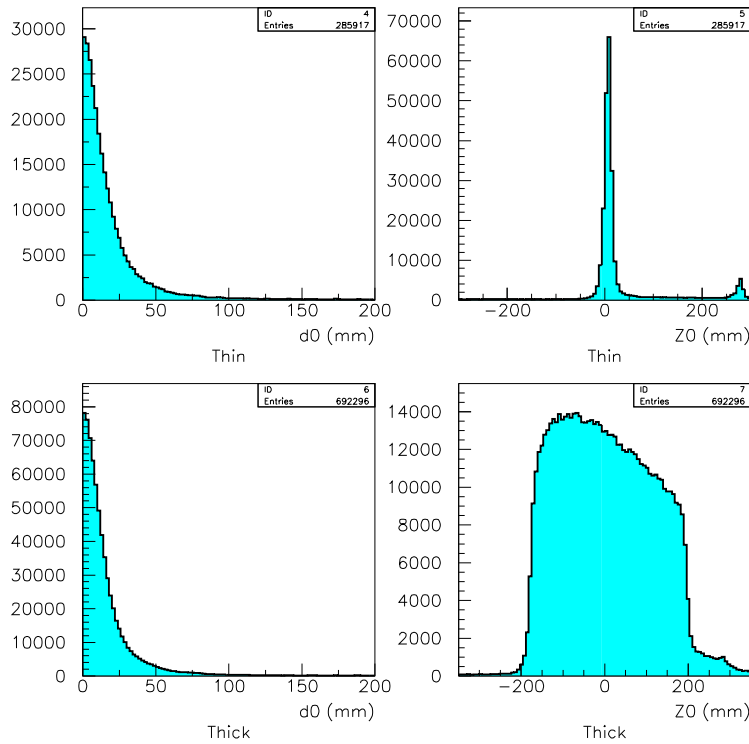

Figure 13.12: Absolute value of the radial coordinate and longitudinal coordinate of the impact point for proton collisions on Al thin (upper plots) and thick (lower plots) target at $12.9\,\mathrm{GeV/c}$ beam momentum.

distributions have a Gaussian shape, and seem not to show the pathologic excess observed in the Tantalum data. This is both due to the software improvement, and
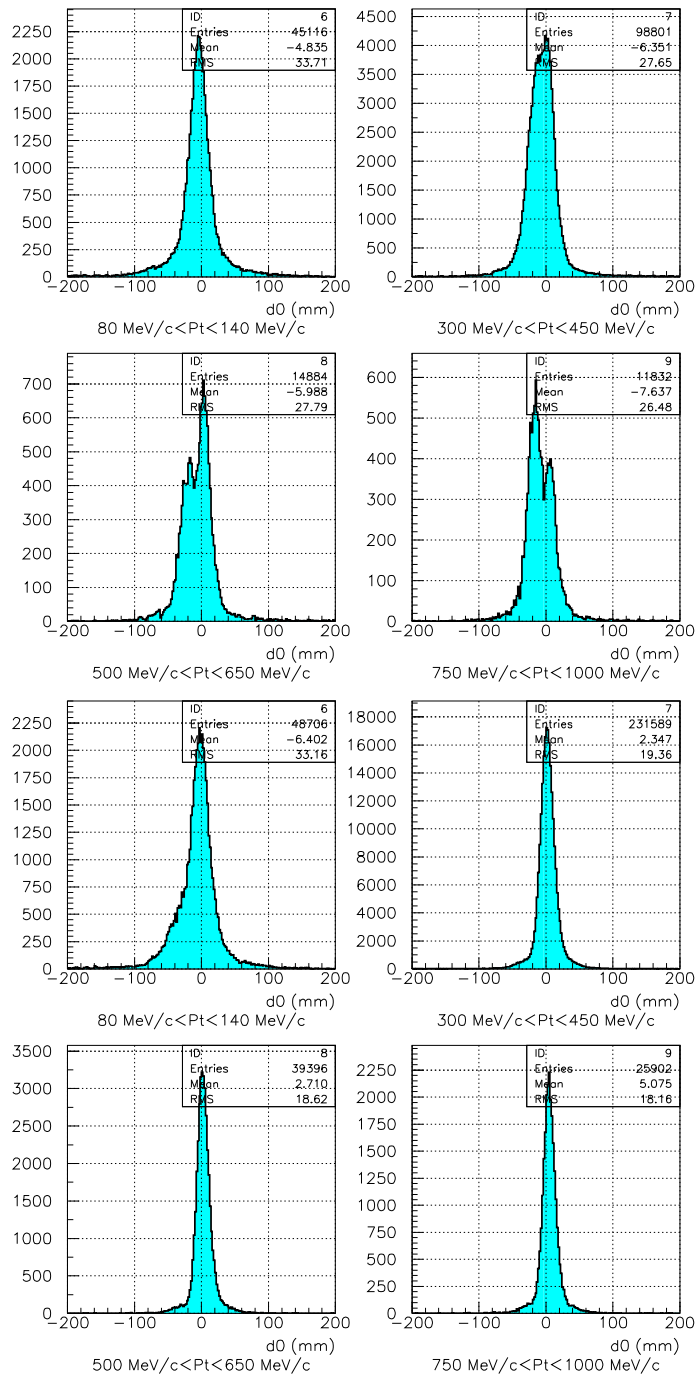
Figure 13.13: Impact parameter at different P_t values for negative (upper 4 plots) and positive (lower 4 plots) particles.

202

to the fact that the data sample is of the 2002 run, when the number of "dead" pads substantially decreased. The z distributions reproduces well the target dimensions. The shape for the thick target reflects the beam attenuation in z due to the interactions. At $z \approx 300\,\mathrm{mm}$, the peak due to interactions in the Stesalite is observed: in the following analysis, a cut on z filters out those events.

A more accurate analysis of the d_0 distributions shows that, at high transverse momentum, when the measurement of the sagitta becomes more critical, the charge assignment problem is still present, especially for negative particles, as shown in figure 13.13. The impact parameter histograms show the superposition of two distributions: a first one, peaked at zero, and relative to events correctly reconstructed, and a second one, shifted towards negative d_0 values. This second component becomes more and more evident with the increasing of the transverse momentum. The problem affects only a small fraction of events with respect to the Tantalum case, as can be also observed comparing figure 13.14, in which d_0 is presented as a function
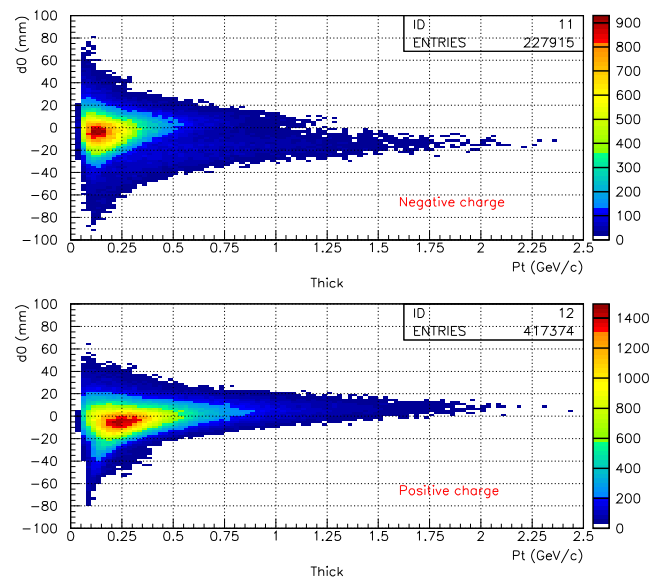

Figure 13.14: Impact parameter as a function of the transverse momentum.

of the transverse momentum, with figure 13.4.

13.6.2 Momentum distributions

In order to compare the momentum distribution with those obtained in the Tantalum case, the same cut on d_0 has been applied. The mean transverse momentum is around $410\,\mathrm{MeV/c}$ while the longitudinal one is around $400\,\mathrm{MeV/c}$. Transverse and longitudinal distributions, shown in figure 13.15 and 13.16, are within the expected
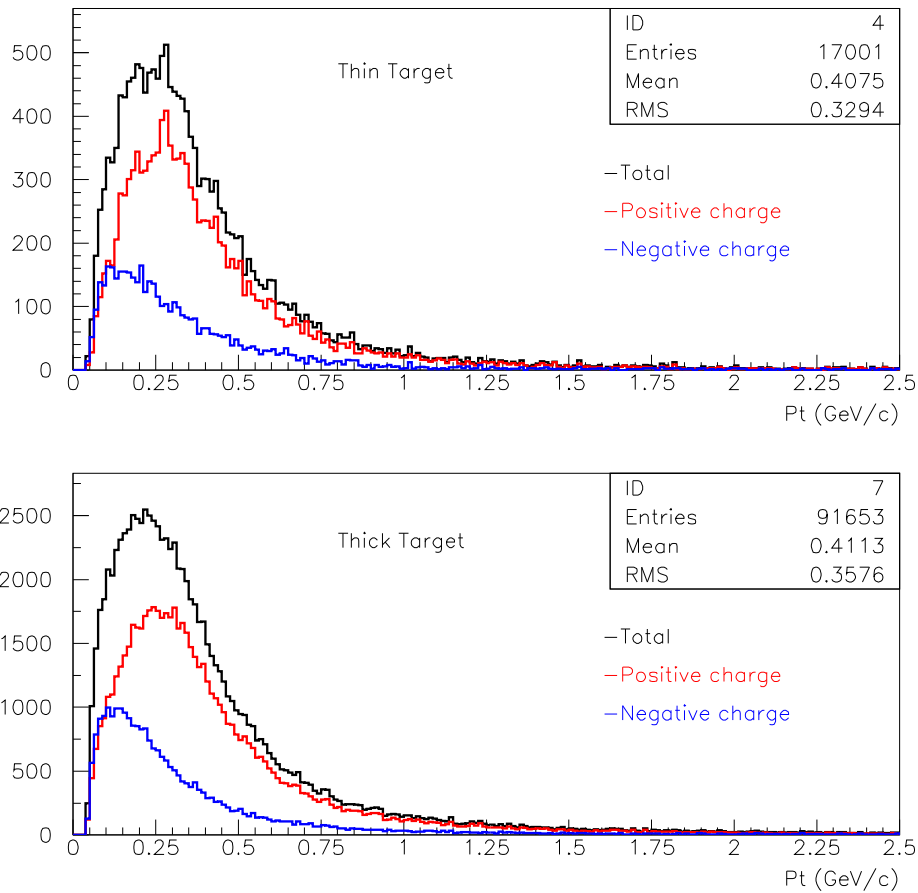

Figure 13.15: Transverse momentum distributions for the Al targets and beam momentum of $12.9\,\mathrm{GeV/c}$.

kinematics bounds and both present a change with momentum of the fractions

of positive and negative particles. As in the previous cases, they suggest that low momentum particles stem mainly out of pair production. The positive to negative particles ratio, integrated over all momenta, is found to be 2.7 for the thin target and 2.5 for the thick one.

The transverse-longitudinal momentum correlation in figure 13.17 is confined by the
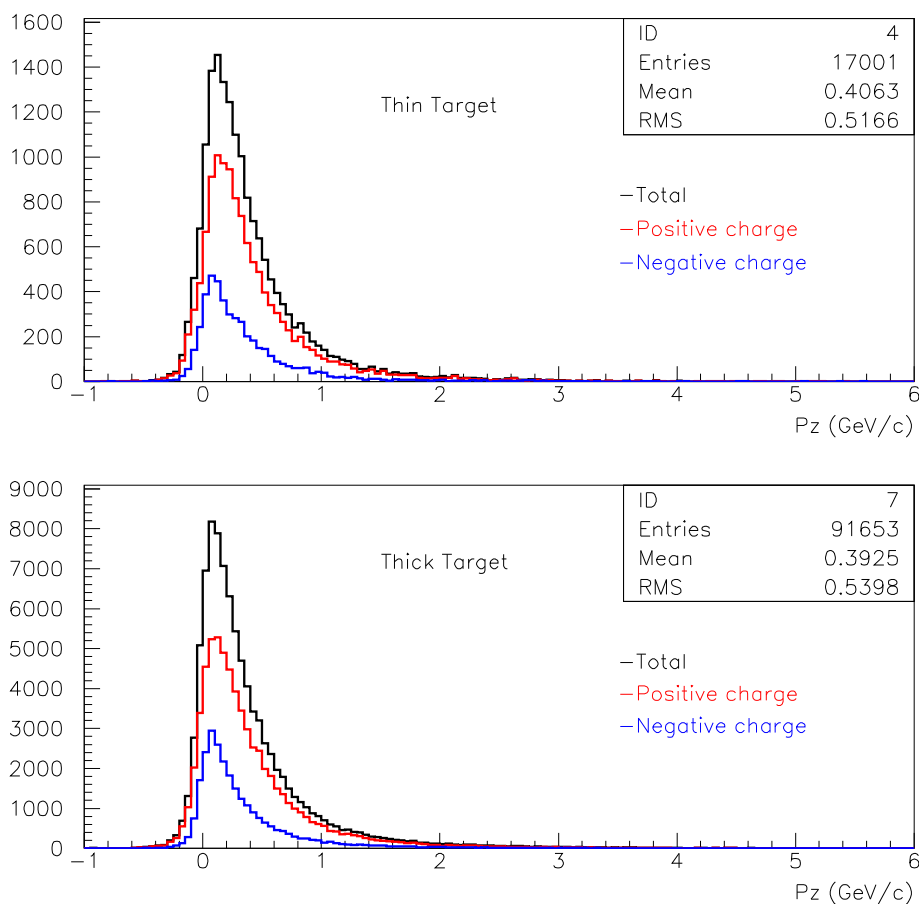

Figure 13.16: Longitudinal momentum distributions for the Al targets and beam momentum of $12.9\,\mathrm{GeV/c}$.

curves dictated by the angular cuts: large values of p_t/p_z are only visible with the statistics of the thick run.

At first sight, there are no major problems in the $12.9\,\mathrm{GeV/c}$ run and there is an

205
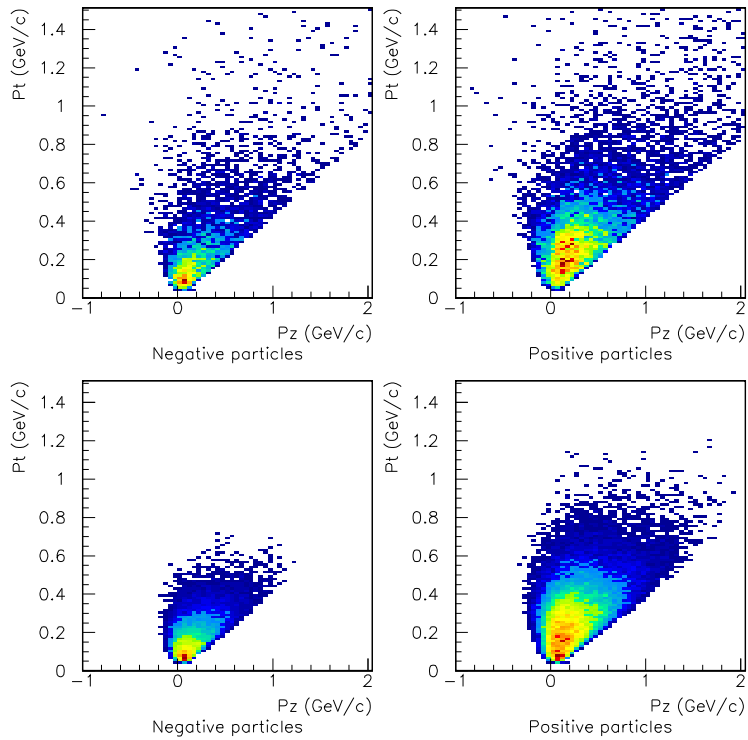
Figure 13.17: Transverse momentum as a function of the longitudinal momentum for thin (upper plots) and thick (lower plots) Al target and proton beam momentum of 12.9 GeV/c.

overall better quality of the data when compared to the tantalum case.

Unfortunately, no further and deeper investigation of these data is possible as long as all the needed software algorithms are implemented and the final calibrations of several relevant part of the detector are completed.

Merci!

Je tiens à remercier très particulièrement le Prof. Allan Clark qui m'a donné la possibilité de travailler à l'Université de Genève et de commencer mon travail de thèse dans une expérience qui représente un vrai défi pour le futur, comme ATLAS. Il a toujours été un énorme soutien pour moi et un guide efficace.

Je remercie le Prof. Alain Blondel, avec qui j'ai pu travailler dans la deuxième partie de ma thèse. Son enthousiasme pour la rechèrche a toujours représenté un exemple pour moi.

Je remercie le Dr. Jaap Panman et le Prof. Martin Pohl pour avoir accepté avec gentillesse de participer à mon Jury.

Merci à Didier qui a guidé avec patience mes premiers pas dans la salle blanche...

Merci à Catherine et à Peggy, qui, en souriant, m'ont constamment aidé avec mes problèmes "bourocratiques".

Merci à tous les collègues qui ont été gentils avec moi et qui m'ont soutenue avec leur chaleur.

Merci à Gersande pour la belle amitié commencée à Londres, et pour avoir corrigé avec patience mon Français.

Merci à Federica, qui a partagé avec moi le bureau, mes joies et mes angoisses. Je me souviendrai de nos "pauses tisane", et pas seulement...

Merci à Christine, pour son amitié profonde, pour ses conseils et pour son encouragement quotidien...

Merci à Salvatore, qui a toujours répondu avec patience à toutes mes questions, posées

à n'importe quel moment...

Merci à Roberto pour sa présence constante, même depuis Rome, et pour son soutien sans faille et son encouragement. C'est grâce à lui que j'ai pu surmonter les moments difficiles des derniers temps.

Merci à mes parents, pour leur amour.

Bibliography

[1] ATLAS Collaboration *ATLAS Technical Proposal* **CERN/LHCC/94-43** (1994)

[2] ATLAS Inner Detector Collaboration *ATLAS Inner Detector Technical Design Report* **ATLAS TDR 4, CERN LHCC 97-16** (1997)

[3] K.G. McKay *Phys.Rev.* **84** (1951) 829.

[4] J. Kemmer *Nuc. Inst. Meth.* **169** (1980) 499.

[5] S.M. Sze *Physics of Semiconductor Devices.* 2nd edition J.Wiley and Sons (1981).

[6] J. Millman *Circuiti e sistemi microelettronici.* Boringhieri (1985).

[7] W.R. Leo *Techniques for Nuclear and Particle Physics Experiments* Springer-Verlag (1987).

[8] C. Posch *Analog readout fot the ATLAS Semiconductor Tracker* (1998).

[9] J. Kemmer *Nuc. Inst. Meth.* **226** (1984) 89.

[10] S. Roe, P. Weilhammer *ATLAS internal note* **ATLAS-INDET 41** (1994).

[11] A. Bar-Lev *Semiconductors and electronic devices* 2nd edition Prentice Hall International (1984).

[12] G. Lutz *Semiconductors Radiation Detectors* Springer (1999).

[13] L. Evensen et al. *Nuc. Inst. Meth.* **A 337** (1993) 44.

[14] G.A. Beck et al. *Nuc. Inst. Meth.* **A 396** (1997) 214.

[15] C.J.S. Damerell, *Vertex Detectors* **RAL 86-77** (1986).

[16] E. Gatti and P.F. Manfredi *La rivista del nuovo cimento* **Vol.9, Serie 3, n°1** (1986).

[17] V. Radeka *Ann. Rev. Nucl. Part. Sci.* **38** (1988) 217.

[18] R. Hofmann et al. *Nuc. Inst. Meth.* **225** (1984) 601.

[19] E. Nygard et al. *Nuc. Inst. Meth.* **A301** (1991) 506.

[20] E. Borchi and M. Bruzzi *La rivista del nuovo cimento* **Vol.17, Serie 3,n°11** (1994).

[21] J. Koutsky and J. Kocik *Radiation damage of structural materials* Elsevier (1994).

[22] J.W. Corbett et al. *Phys. Rev. A* **138** (1965) 555.

[23] T.P. Ma et al. *Ionizing Radiation effects in MOS Devices and Circuits* J.Wiley and Sons (1989).

[24] T. Shulman **HU-SEFT 1991-07** (1991).

[25] E. Barberis et al. *Nuc. Inst. Meth.* **A326** (1993) 373.

[26] F. Lemeilleur et al. *Nuc. Inst. Meth.* **A360** (1995) 438.

[27] The ROSE collaboration *RD 48 Status Report* **CERN/LHCC 39** (1997).

[28] D. Pitzl et al. *Nuc. Inst. Meth.* **A311** (1992) 98.

[29] H.J. Ziock et al. *IEEE Trans. Nucl. Sci.* **40** (1993) 344.

[30] H.J. Ziock et al. *Nuc. Inst. Meth.* **A342** (1994) 96.

[31] SCT Detector Collaboration *ATLAS internal note* **SCT/Detector FDR** (1999).

[32] A. Peisert *Delphi internal note* **92-143 MVX 2** (1992).

[33] P. Horowitz and W. Hill *The Art of Electronics* Cambridge University Press (1989)

[34] G. Lindstrom *SITP internal note* **SITP-002** (1991).

[35] V. Cindro et al. *Nuc. Inst. Meth.* **A439** (2000) 337.

[36] E. Belau et al. *Nuc. Inst. Meth.* **214** (1983).

[37] E. Chesi et al.*IEEE Trans. Nucl. Sci.* **47** (2000) 1434.

[38] J. Kaplon et al.*Fifth Workshop on Electronics for LHC Experiments, Snowmass September 20-24,1999* **CERN/LHCC/99-33** (1999).

[39] ATLAS Inner Detector Collaboration *Extract from contractual documents* **ATLAS SCT/Detector PRR/00-1** (2000)

[40] Z. Li and H.W. Kraner *IEEE Trans. Nucl. Sci.* **38** (1991) 244.

[41] D. Ferrere and M.C. Morone *Measurements of CSEM detectors for qualification in the ATLAS experiment* **ATLAS SCT/Detector Note** (1999)

[42] ATLAS Inner Detector Collaboration *ATLAS Detector measurements* **ATLAS SCT/Detector FDR/99-8** (1999)

[43] The HARP Collaboration *Proposal to study hadron production for the ν factory and for the atmosferic ν flux* **CERN-SPSC/99-35** (1999)

[44] J. Collot et al. *Nuc. Inst. Meth.* **A 451** (2000) 327.

[45] T. Abbott et al. *Phys. Rev.* **D 45** (1992) 3906.

[46] N. Cabibbo *Phys. Rev. Lett.* **10** (1963) 531.

[47] M. Kobayashi and T. Maskawa *Prog. Theor. Phys.* **49** (1973) 652.

[48] B. Kayser *Phys. Rev.* **D66** (2002) 392.

[49] V.M. Lobashev et al. *Phys. Lett.* **B460** (1999) 227.

[50] S. Pascoli et al. **hep-ph/0212113 v2** (2002).

[51] The SNO Collaboration **nucl-ex0204009** (2002).

[52] The KamLAND Collaboration **hep-ex/0212021 v1** (2002).

[53] M. Apollonio et al. *Phys. Lett.* **B466** (2002) 415.

[54] F. Boehm et al. *Phys. Rev.* **D64** (2001) 112001.

[55] G.L. Fogli et al. *Phys. Rev.* **D66** (2002) 010001-406.

[56] E. Kearns *Proc of the 30th Int. Conf. on HEP* (2001) 172.

[57] T. Kajita *Talk at 18th Int. Workshop on Weak Interactions and Neutrinos* (2002).

[58] K. Nishikawa *Talk at XXth Int. Conf. on Neutrino Physics and Astrophysics* (2002).

[59] The LEP Collaborations **hep-ex/0212036** (2002)

[60] The LSND Collaboration *Phys. Rev.* **D 64** (2001) 112007.

[61] M. Apollonio et al. *Oscillation physics with a neutrino factory* **CERN-TH/2002-208** (2002).

[62] The HARP Collaboration *Status Report of the HARP experiment* **CERN-SPSC/2002-13** (2002).

[63] The NOMAD Collaboration *Nuc. Inst. Meth.* **A404** (2002) 96.

[64] J. Dumarchez *Talk at the HARP General Meeting 10/6/02* (2002).

[65] The CHORUS Collaboration *Nuc. Inst. Meth.* **A349** (1994) 70.

[66] The CHORUS Collaboration *Nuc. Inst. Meth.* **A378** (1996) 221.

[67] C. Valli *Tesi di laurea* (2001).

[68] The HARP Collaboration *Status Report of the HARP experiment* **CERN-SPSC/2001-031** (2001).

[69] F. Bobisut et al. *HARP Note* **02-007** (2002).

[70] F. Bonesini et al. *HARP Note* **02-004** (2002).

[71] C. Booth *HARP Note* **02-006** (2002).

[72] A. Grossheim *Private Communication* (2002).

[73] The HARP Collaboration *Status Report of the HARP experiment* **CERN-SPSC/2002-19** (2002).

[74] The ALICE DAQ Group *ALICE Note* **ALICE99/46** (1999).

[75] W. Blum and L. Rolandi *Particle detection with Drift Chambers* **Springer** (1994).

[76] C. Grupen *Particles detectors* (1996).

[77] E. Gatti et al. *Nuc. Inst. Meth.* **163** (1979) 83.